IEEE Transactions on Nuclear Science, Vol. NS-26, No. 3, June 1979

ELECTRON RING ACCELERATOR RESEARCH AT THE UNIVERSITY OF MARYLAND†

C. D. Striffler, R. A. Meger, J. Grossmann, E. Pappas,
M. Reiser, M. J. Rhee, T. F. Wang

Abstract

The feasibility of forming E rings by injecting a hollow beam through a static cusped magnetic field is being investigated in the University of Maryland ERA project. Recently, we demonstrated the trapping of such rings using a resistive wall in conjunction with a static magnetic mirror. This paper presents studies with a time varying mirror coil so that reacceleration of the ring after trapping can be examined. Results concerning the coherent motion of the rings and axial focusing due to an inner squirrel cage conductor are presented. Based on these results, design studies for the next stage of the UMERA system are discussed.

1. Introduction

Since the last Particle Accelerator Conference,[1] the University of Maryland ERA (UMERA) project has been concerned with various effects relative to forming electron rings using a cusp-injected electron beam configuration.[2-4] During this period, we demonstrated the trapping of the cusp-injected beam using a surrounding resistive wall in conjunction with a static magnetic mirror well.[3] In this paper, we present studies where the static mirror coil is replaced by a time varying mirror coil (TVMC).

The UMERA system is schematically shown in Fig. 1. The 2.5 MeV annular beam from a 12 cm diameter knife-edged cathode passes through a cusped magnetic field which transforms a substantial portion of its axial velocity into azimuthal velocity. Entering the downstream region, the rotating beam has a mean radius of 6 cm, propagates with axial velocity 0.2 c to 0.3 c, has a peak axial current of 1.5 kA, and a 3-5 ns FWHM pulse width. The downstream vacuum region consists of a 15 cm radius wall lined with copper mesh, a resistive wall of radius 7.5 cm, and a squirrel cage conductor located inside of the rotating beam. Besides the main coils that produce the cusp field, a small, 1-turn TVMC (radius 10 cm) is placed 100 cm downstream from the iron plate. The current pulse shape of this coil is approximately a half sine wave of length 300 ns, shown in the inset of Fig. 2(a). This coil can produce a peak field of about 200 G. An axial magnetic field profile is shown in Fig. 2(b) at various times during the TVMC pulse. The main coils provide a flat field region from 20-50 cm and a diverging field beyond 50 cm having a 10% decrease in 150 cm, giving an acceleration B_r field on the average of 3 G for a flat field of 1600 G. For the case shown, the well minimum at peak current is between 75 and 80 cm.

2. Coherent Ring Motion - Theory and Experiment

To understand the coherent motion of the E ring during the slowing down, trapping, and subsequent release of the ring into the acceleration field, we consider the following simplified model. A filamentary ring of radius R containing N_e electrons having azimuthal and axial velocity components $v_\phi = \beta_\phi c$ and $v_z = \beta_z c$, and relativistic mass ratio $\gamma = (1 - \beta_\phi^2 - \beta_z^2)^{-1/2}$ moves close and coaxial to a thin resistive wall of radius R_w and surface resistivity ρ_s Ω/sq.[5] The induced image current decay in the wall produces a retarding force on the ring in the axial direction. In a uniform field B_{zo}, the axial equation of motion can be integrated to obtain the stopping distance L_s of the ring. The result is

$$L_s = m\gamma_o \frac{4\pi}{\mu_o e^2} \frac{2\pi R(R_w - R)}{N_e} \frac{\beta_{zo} + \left[\left(\frac{2\rho_s}{Z_o}\right)^2 + \left(\frac{Z_o}{2\rho_s}\right)^2\right]\frac{\beta_{zo}^3}{3}}{\frac{2\rho_s}{Z_o} + \beta_{\phi o}^2 \frac{Z_o}{2\rho_s}} \quad (1)$$

where $\gamma_o, \beta_{\phi o} = (eB_{zo}/m\gamma_o c)R$, β_{zo} are initial ring parameters and $Z_o = 377\ \Omega$. This expression has two minima in L_s as a function of ρ_s, one representing the maximization of the magnetic stopping force at a low value of ρ_s and the other the electric stopping force. For $\beta_{zo} = 0.2$-0.3, the minima occur near 30 and 1000 Ω/sq, respectively. For our application, only the low-resistivity case is of interest. The range in β_{zo} in our cusp system is necessitated by the strong resistivity of beam energy to magnetic field setting near the cutoff field and the uncertainty in operating diode voltage. Also, due to the cusp system, the rotating beam initially has a highly peaked front end density which gradually spreads out as the ring propagates down the system, thus continually reducing the slowing-down effect of the resistive wall. This means that the stopping distance is longer than that computed by the ideal model. Therefore, in addition to the resistive wall, a magnetic well is formed by a TVMC so as to set up a trapping region.

Using the above described model for the ring-resistive wall and for the applied magnetic fields of the UMERA shown in Fig. 2(b), the ring motion is determined by solving the relativistic equations of motion. A typical result for one set of parameters is shown in a phase-space diagram, β_z vs z, in Fig. 2(a). For this example, the TVMC peak current is 96 A (8 turns) which is superimposed on the main field that has a flat field value of 1665 G. The E ring initial parameters are $\gamma_o = 6$, $R_o = 6$ cm, $\beta_{zo} = 0.134$, and $N_e = 5 \times 10^{11}$, the "effective" number of filamentary ring particles. A value of 30 Ω/sq is used for the wall resistivity. The ring is injected (z = 0) 100 ns into the TVMC pulse. As seen from the figure, the ring is slowed down and trapped in the magnetic well and settles down to the well minimum at about 85 cm after its axial motion is damped. This takes about 100 ns into the ring lifetime. The ring then slowly moves with the well minimum as the coil current decreases. At about 180 ns, the ring is no longer confined by the well configuration and is thus accelerated out of the well into the acceleration region. The ring reaches a speed of about 0.1 c at an axial position of 120 cm. The resistive wall prevents a continual increase in β_z that would occur without it; the asymptotic value is reached when the acceleration B_r field is balanced by the decelerating resistive wall field.

In the UMERA experimental setup, passively integrated magnetic probes are located on axis (see Fig. 1) inside the squirrel cage conductor at axial positions of 75, 85, 95, 110, and 120 cm. The ring motion in a typical shot as seen by these probes is shown in Fig. 3 [$\gamma \simeq 5.5$, $B_{zo} = 1500$ G]. Each plot is the magnetic field registered by the particular probe versus time relative

†Research supported by the National Science Foundation.

*Electrical Engineering Department and Department of Physics and Astronomy, University of Maryland, College Park, Maryland 20742.

0018-9499/79/0600-4234$00.75 © 1979 IEEE

to the firing of the mirror coil. The baseline for the probes, represented by the dashed lines in the figures, represents the TVMC signal which is recorded prior to the firing of the beam. As the figures show, the beam is injected about 100 ns after the firing of the coil. The ring arrives at the 75 cm probe, passes by it, and is reflected off the mirror field formed by the TVMC. The ring is trapped and performs approximately a simple harmonic oscillation about the well minimum with a period of 25-30 ns. As the TVMC current decreases, the mean position of the ring moves downstream. The change in frequency on the 75 cm probe signal indicates that the E ring is no longer centered about the 75 cm probe location. During this trapped regime, the axial motion of the ring is continually damped by the resistive wall interaction. As the ring moves closer to the mirror location, the particles start to escape over the mirror field. Eventually the entire ring spills out of the well and the probe signals decrease to zero. The 110 and 120 cm probes, downstream of the TVMC, see the accelerated ring as it passes by. The peak beam signal has decreased and has slightly spread out. A comparison shows that there is good qualitative agreement between these experimental observations and the theoretical results presented in Fig. 2.

Other areas of agreement between the model and the experiment are briefly discussed. Firstly, experiments were performed with different resistive walls. As predicted by the model, the best results are obtained with walls of 30-50 Ω/sq. Secondly, experiments were performed with different anode foils through which the beam passes. In general, the foil is needed to reduce the destructive effects of the negative mass instability. However, in the cusp-injected system, the foils produce a spread in axial velocity that reduces the front end density peaking of the ring. This in turn reduces the resistive wall retarding force. Thus, an optimal foil thickness is required to achieve an acceptable compromise between these two effects. Best results are obtained with a 0.25 mil mylar foil.

For future experiments to load positive ions into the electron ring, we have built a puff valve that injects a well-localized gas cloud into the system. The valve is located inside the squirrel cage and can be moved to different axial positions. We have started some initial experiments to investigate the effects of the neutral gas on the coherent motion of the ring. Preliminary data with hydrogen gas and with the puff valve located at 50 cm downstream from the cusp, show a distinct damping of the coherent axial oscillations in the time-varying mirror field. With no gas from the puff valve, at a vacuum background density (air) of $n \sim 10^{12}$ cm^{-3}, we observe an initial decrease in the probe signal over 40 ns followed by almost undamped oscillations until the ring spills out of the mirror (~150 ns later). With the presence of hydrogen gas from the puff valve, the oscillations are damped with a time constant that decreases with gas particle density. Typically, for hydrogen density of $n \sim 10^{15}$ cm^{-3}, this damping is almost instant, i.e., the ring settles down immediately and shows no coherent oscillation until spillout occurs. A theoretical analysis of the axial deceleration of an electron ring interacting with a gas cloud was presented in a recent paper which gives a good qualitative picture of this process.[6]

3. Focusing Effects - Incoherent Motion

During the various stages of ring evolution, the ring must be radially and axially focused in order to maintain its coherence. A small amount of space-charge neutralization, applied magnetic field profile change, and/or appropriate arrangement of surrounding conducting walls can provide the required focusing to overcome the "net" relativistic $(1-\beta^2)$ defocusing effect. In other words, a minimum particle γ exists below which focusing does not occur.

The focusing problem is most critical when the ring is in a uniform magnetic field with no space-charge neutralization, and thus conducting walls must provide the required axial focusing. To delineate the minimum γ effect for the conducting wall case, consider the Cartesian geometry model of the E ring shown in Fig. 4. The ring has a length L, a thickness T, a uniform density, and a mean velocity βc directed out of the figure. The mean position of the ring is a distance h from the squirrel cage (S.C.) conductor, which allows image space charges but no image currents. For this model, it is straightforward to calculate the total electric and magnetic fields at the ends of the ring. To obtain a net focusing effect, the axial force $F_z = q(E_z - \beta c B_x)$ at this position must be less than zero. The calculations show that in this case the relativistic mass factor γ must be greater than the critical value

$$\gamma_c = \left[\frac{t \ln\left(1+\frac{1}{t^2}\right) + 2\tan^{-1} t}{s \ln \frac{U}{V} + \frac{t}{2} \ln UV + \tan^{-1}\left(\frac{2t}{1+4s^2-t^2}\right)} \right]^{-1/2}, \quad (2)$$

where $s = h/L$, $t = T/2L$, $U = 1 + 1/(2s+t)^2$ and $V = 1 + 1/(2s-t)^2$. As an example, if $T/L = 1/5$ and $T/h = 1$, we find from Eq. (2) that $\gamma > \gamma_c = 2$ is required for axial focusing. However, if $T = L = h$, then $\gamma > \gamma_c = 10$ is required for focusing unless, of course, the ring is brought closer to the S.C.

In the present UMERA system, the ring properties are $N \simeq 10^{13}$ particles, $T \simeq 3$ cm, $L \simeq 15$ cm, and $\gamma \simeq 5.5$, and the surrounding walls consist of the inner S.C. and outer resistive wall. Using cylindrical geometry but otherwise the same type of model as shown in Fig. 4, i.e., uniform density, we find that an inner S.C. conductor provides axial focusing; however, without an inner S.C., the ring is axially defocused if the beam is too far from the outer resistive wall which acts as a S.C.

This focusing effect of an inner squirrel cage has been studied experimentally, and the results for three geometries are shown in Fig. 5. In one case, no S.C. is present, whereas in the other cases, 8 and 16 copper strips are placed equally about a radius of 2.5 cm. In this figure, the peak signals from the magnetic probes are plotted versus the probe position. All signals are normalized to the 85 cm, 16 conductor case. One point to note is that the S.C. plays an important role in the amount of trapped beam, with more conductors implying more trapped ring particles. This effect is believed to be due to the S.C. maintaining a relatively shorter and more densely-peaked beam from injection through the slowing down and trapping process, thus increasing the resistive wall retarding effect.

Another point to note from Fig. 5 is that a larger fraction of the E ring survives with an inner S.C. beyond the TVMC, an asymptotic effect being achieved with 8 or 16 strips. The loss of peak signal after release of the ring from the trapping region can be explained by the fact that the ring does not remain axially focused due to the strong B_r field of the TVMC and the diverging main field. The S.C. provides focusing which counteracts this effect. However, the B_r fields due to the TVMC and the main field are at some places as large as 6 G, which is sufficient to

overcome the S.C. focusing forces. Modifications to the present system to alleviate this undesirable effect are discussed in the next section.

4. Conclusions and Future Considerations

The processes leading to the trapping and reacceleration of the E ring in the present UMERA system composed of a resistive wall, an inner S.C., and a TVMC have been presented. The trapped ring is axially focused by electric-image boundaries and has a surface electric field at the ends around 1 MV/m. However, the studies presented here indicate that the strong B_r field due to the TVMC that the ring experiences upon release from the trapping region is sufficient to cause defocusing. To alleviate the defocusing features of the present system, we have considered a modification to our ERA system which is depicted by the axial magnetic field plot as a function of time shown in Fig. 6. Specifically, the axial magnetic field is plotted versus axial position at various times during the ring motion. The trapping region is formed by the main magnetic coils (t = 0 plot) with the well minimum located at about 80 cm. The main coil field peaks at about 110 cm with the acceleration region thereafter adjusted to have a slope consistent with holding an ion in a ring with 1 MV/m surface electric field. After the ring is trapped in the well region, three TVMC's are sequentially turned on and move the ring up the mirror field and into the acceleration region. The positions, time sequences, and currents of the three TVMC's, identical to those used in the present UMERA, are given in the inset table of Fig. 6. The advantages of this design are obvious with respect to axial focusing; that is, the front of the ring does not see a radial magnetic field much greater than the value in the acceleration region. The ring can be loaded with ions during the relatively slow pushing process. Ultimately, this system must include adiabatic compression to reduce the minor cross section of the ring and thus lead to larger holding powers.

References

1. W. W. Destler et al., IEEE Trans. Nucl. Sci. 24, 1656 (1977).
2. R. A. Meger et al., and C. D. Striffler et al., Proc. 2nd Int. Topical Conf. on High Power Electron and Ion Beam Res. & Tech., Cornell U., Ithaca, N.Y., pp. 601 and 481 (1977).
3. D. W. Hudgings et al., Phys. Rev. Lett. 40, 764 (1978).
4. C. D. Striffler et al., and R. A. Meger et al., 3rd Int. Conf. on Collective Methods of Acceleration, May 22-25, Laguna Beach, Calif., 1978, to be published in the proceedings.
5. P. Merkel, Part. Accel. 8, 21 (1977).
6. U. Schumacher et al., Part. Accel. 7, 245 (1976).

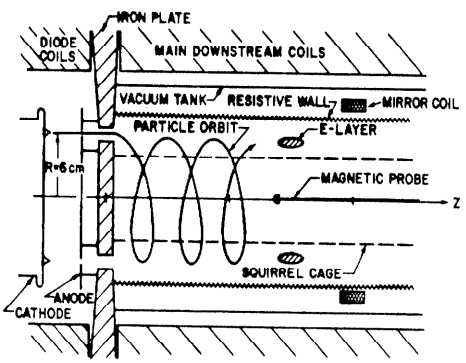

Fig. 1 Schematic of the UMERA system.

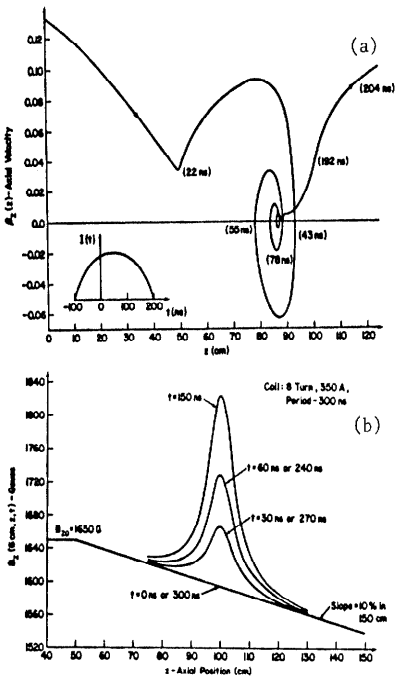

Fig. 2 (a) "Ring" phase-space motion. Ring parameters: $\gamma_o = 6$, $R_o = 6$ cm, $\beta_{zo} = 0.134$, and $N_e = 5 \times 10^{11}$. Resistive wall: $R_w = 7.5$ cm, $\rho_s = 30\ \Omega$/sq. TVMC: 96 A, 8 turns. (b) Axial magnetic field profile with the TVMC with time t a parameter.

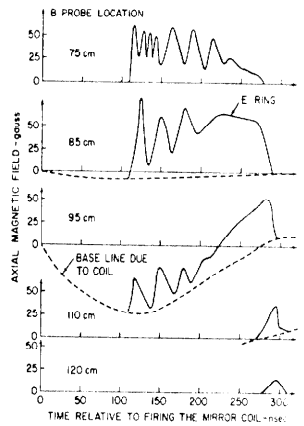

Fig. 3 Axial magnetic field probe measurements versus time relative to firing of the TVMC. Data from five B probes at different axial positions are shown. The TVMC is centered at 100 cm. The dashed lines represent only the TVMC, the solid lines the TVMC plus the E ring.

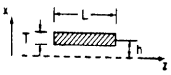

Fig. 4 Cartesian model for the E ring-squirrel cage axial focusing mechanism.

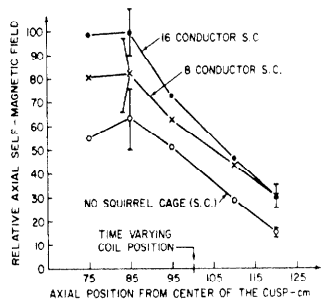

Fig. 5 Relative ring self magnetic field data versus probe location for different inner S.C. configurations. Each data point represents an average of 5 or more shots.

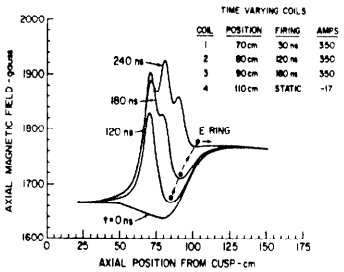

Fig. 6 Axial magnetic field profile at various times during a pushing scheme for future UMERA experiments. Three TVMC's are used in conjunction with a rearrangement of the main field coils.